Journal of Power Sources 195 (2010) 6239–6244

Contents lists available at ScienceDirect

Journal of Power Sources

journal homepage: www.elsevier.com/locate/jpowsour

Preparation and characterization of Ni-based positive electrodes for use in aqueous electrochemical capacitors

Hiroshi Inoue*, Yusuke Namba, Eiji Higuchi

Department of Applied Chemistry, Graduate School of Engineering, Osaka Prefecture University, 1-1, Gakuen-cho, Sakai, Osaka 599-8531, Japan

ARTICLE INFO

Article history:
Received 16 October 2009
Received in revised form
24 November 2009
Accepted 4 December 2009
Available online 8 January 2010

ABSTRACT

We have prepared NiO particles on Ni sheet and Ni foam substrates by chemical bath deposition and the following heat-treatment, and assembled a hybrid capacitor (HC) cell with the NiO-loaded Ni sheet or Ni foam positive electrode and activated carbon negative electrode. The deposited NiO particles had flower-like porous morphology which was composed of aggregated nanosheets. The maximum operating voltage of both HC cells was 1.5 V, which was much higher than theoretical decomposition voltage of water (1.23 V). The HC cell with NiO/Ni foam (HC_{foam}) had higher discharge capacitance and high-rate dischargeability and lower IR drop than the HC cell with NiO/Ni sheet (HC_{sheet}) because of the increase in the utilization of NiO active material. Both energy and power densities per mass of active materials, were much higher than those for the HC_{sheet}. Both HC_{foam} and HC_{sheet} showed excellent cycle stability for 2000 cycles.

1. Introduction

Aqueous electrolytes have advantages such as high ionic conductivity, nonflammability, low environmental load, low cost etc. compared to nonaqueous electrolytes [1]. However, the maximum operating voltages of electric double layer capacitors (EDLCs) with aqueous electrolyte solutions are much lower than those with nonaqueous electrolyte solutions which operate at voltages over 2.5 V because the former is limited to 1.23 V, the theoretical decomposition voltage of water, leading to low energy density. A key to higher energy density is to raise the maximum operating voltage and capacitance. Recently, aqueous hybrid capacitors (HCs) which are composed of an activated carbon (AC) electrode and an oxide electrode with pseudocapacitance have been developed, and energy density was improved significantly because of the increased maximum operating voltage and capacitance compared to the EDLCs [2–11]. Ni hydroxide and oxide [5,6], CoAl double hydroxides [7], manganese oxides [8–11] etc. as a positive electrode material and zinc as a negative electrode material [12] have realized maximum operating voltages of 1.4–2.0 V, because their operating potential range is outside of that of the AC electrode. In addition, they have higher oxygen or hydrogen overpotential than AC, leading to higher energy density. Recently, we have assembled an HC with a sintered $Ni(OH)_2$ positive electrode used for commercial Ni/MH batteries and succeeded in the increase in operating voltage [6]. In the charge–discharge curves of the HC, the potential of the AC negative electrode cycled in a wide potential range, while that of the sintered $Ni(OH)_2$ positive electrode scarcely moved during charging and discharging. So it seems difficult to increase the cell voltage more and more. To increase the operating voltage, the potential of the positive electrode should cycle in wider potential ranges. We have assembled an HC cell with nickel oxide positive electrode prepared by the heat-treatment of the sintered $Ni(OH)_2$, and succeeded in the increase in operating voltage and capacitance, leading to the higher energy and power densities [13]. The sintered $Ni(OH)_2$ electrode is available for commercial Ni/MH batteries because of high packing density of $Ni(OH)_2$ particles. But, the higher the packing density, the smaller the interface area between the particles and electrolyte solution, leading to lower capacitances per weight of active material and lower rate capabilities. So the sintered $Ni(OH)_2$ electrode with too much high packing density of active material seems to be undesirable for the capacitor use.

Chemical bath deposition (CBD) is a simple preparation method having advantages of low cost, room temperature technique, large surface area of deposits and so on, and several researchers have reported the preparation of some hydroxides by this method [14–19]. In this study, we assembled HCs with NiO particles prepared on different Ni substrates by the CBD method and the following heat-treatment, as a positive active material, and investigated their charge–discharge properties.

* Corresponding author. Tel.: +81 72 254 9283; fax: +81 72 254 9283.
E-mail address: inoue-h@chem.osakafu-u.ac.jp (H. Inoue).

0378-7753/$ – see front matter © 2009 Elsevier B.V. All rights reserved.
doi:10.1016/j.jpowsour.2009.12.018

2. Experimental

2 mL of ammonia water (25%) was slowly put in a beaker with 8 mL of 1 M nickel sulfate aqueous solution at 30 °C. Then 10 mL of 0.15 M potassium persulfate aqueous solution was added into the beaker, followed by stirring for 3 min. The resultant solution is named a CBD bath hereafter.

Two types of Ni substrates, a Ni sheet and Ni foam, were used in this study. The nickel sheet (15 mm × 10 mm × 0.2 mm) was soaked in the CBD bath at 30 °C for 90 min, while the nickel foam (30 mm × 10 mm × 1.6 mm) was done at the same temperature for 15 min. Then the Ni sheet or Ni foam with deposits was washed by ultrapure water and dried in a desiccator at room temperature, followed by heat-treating at 400 °C for 1 h. The amount of deposits on the Ni sheet and Ni foam was evaluated from the difference between total mass before and after the CBD.

X-ray diffraction spectra of deposits on the Ni sheet or Ni foam were measured by using an X-ray diffractometer equipped with a Cu Kα source (λ = 0.1541 nm, 50 kV, 30 mA). The surface morphology of the deposits was analyzed using a field-emission scanning electron microscope (FE-SEM, Hitachi S-4500) for higher magnification and a scanning electron microscope (Keyence VE-9800) for lower magnification. Elemental analysis of the deposits was carried out with a detector for energy dispersive X-ray spectroscopy (EDX) equipped with the latter microscope.

The sintered $Ni(OH)_2$ electrode (10 mm × 9 mm × 0.7 mm), which had been also used in Ref. [6], was used for reference in this study. The sintered $Ni(OH)_2$ electrode was heat-treated at 350 °C for 1 h to be transformed to NiO. The resultant electrode is named NiO(sintered) hereafter. The mass of the active material was measured after it was carefully scratched out from the substrate.

The preparation of an activated carbon (AC) negative electrode and the fabrication of an HC cell were performed according to Ref. [6]. The reference electrode and electrolyte were the Hg/HgO electrode and 10 M KOH aqueous solution. Cyclic voltammograms of various positive electrodes were measured at 20 mV s^{-1}. Charge–discharge cycle tests were done by charging up to 1.5 V at 1 mA and discharging down to 0.8 V at the same current. Discharge capacitance (C_{dis}) specified as a gravimetric value is evaluated from the following Eq. (1):

$$C_{dis}\,[F\,g^{-1}] = \frac{i_{dis}t}{(V_2 - i_{dis}R - V_1)m} \quad (1)$$

where i_{dis}, t, R and m represent discharge current in ampere, discharge time in second, cell resistance in ohm and total mass of active materials at both electrodes in gram, respectively. V_1 and V_2 represent potentials at lower and upper limits, which are 0.8 V and 1.5 V in the present study, respectively. The R-value was evaluated from a voltage drop (ΔV) at the beginning of discharging, that is the IR drop, as follows:

$$R = \frac{\Delta V}{i_{dis}} \quad (2)$$

To get high-rate dischargeability (HRD) for each HC cell, discharge capacities at various currents were measured after charging at 1 mA. Before that, the charge–discharge cycling at 1 mA in the potential range between 0.8 and 1.5 V was repeated 100 times. The HRD value is evaluated from the following equation:

$$HRD\,[\%] = \frac{100C_i}{C_1} \quad (3)$$

where C_i and C_1 represent discharge capacitances at i mA and 1 mA, respectively.

All electrochemical measurements were carried out at 30 °C.

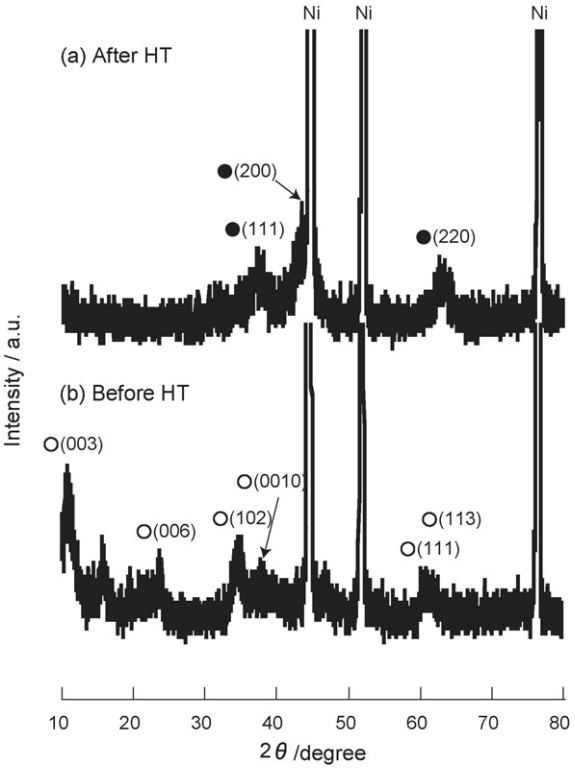

Fig. 1. XRD patterns for deposits prepared on a Ni foam by CBD (a) after and (b) before heat-treatment (HT) at 400 °C for 1 h. (○) $Ni(OH)_2$(OH, S, H_2O); (●) NiO.

3. Results and discussion

Fig. 1 shows XRD patterns for deposits prepared on a Ni foam by CBD ($Ni(OH)_2$(CBD)/Ni foam) before and after heat-treatment

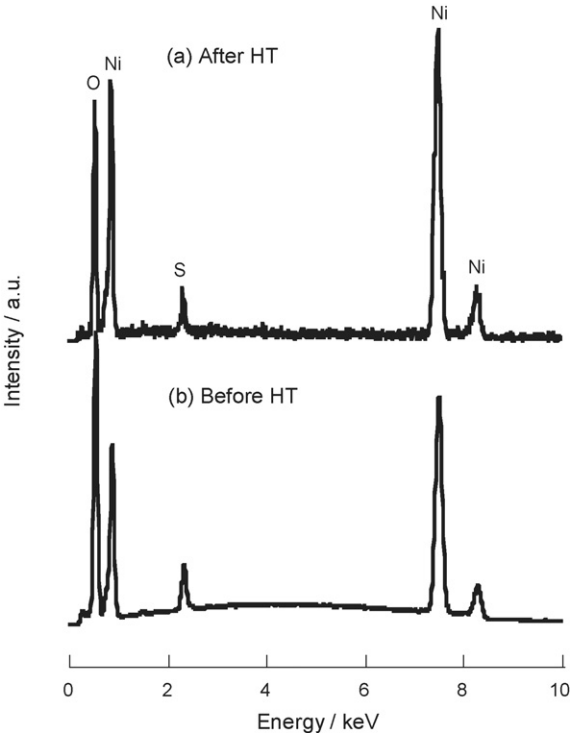

Fig. 2. EDX spectra of deposits prepared on a Ni foam by CBD (a) after and (b) before heat-treatment at 400 °C for 1 h.

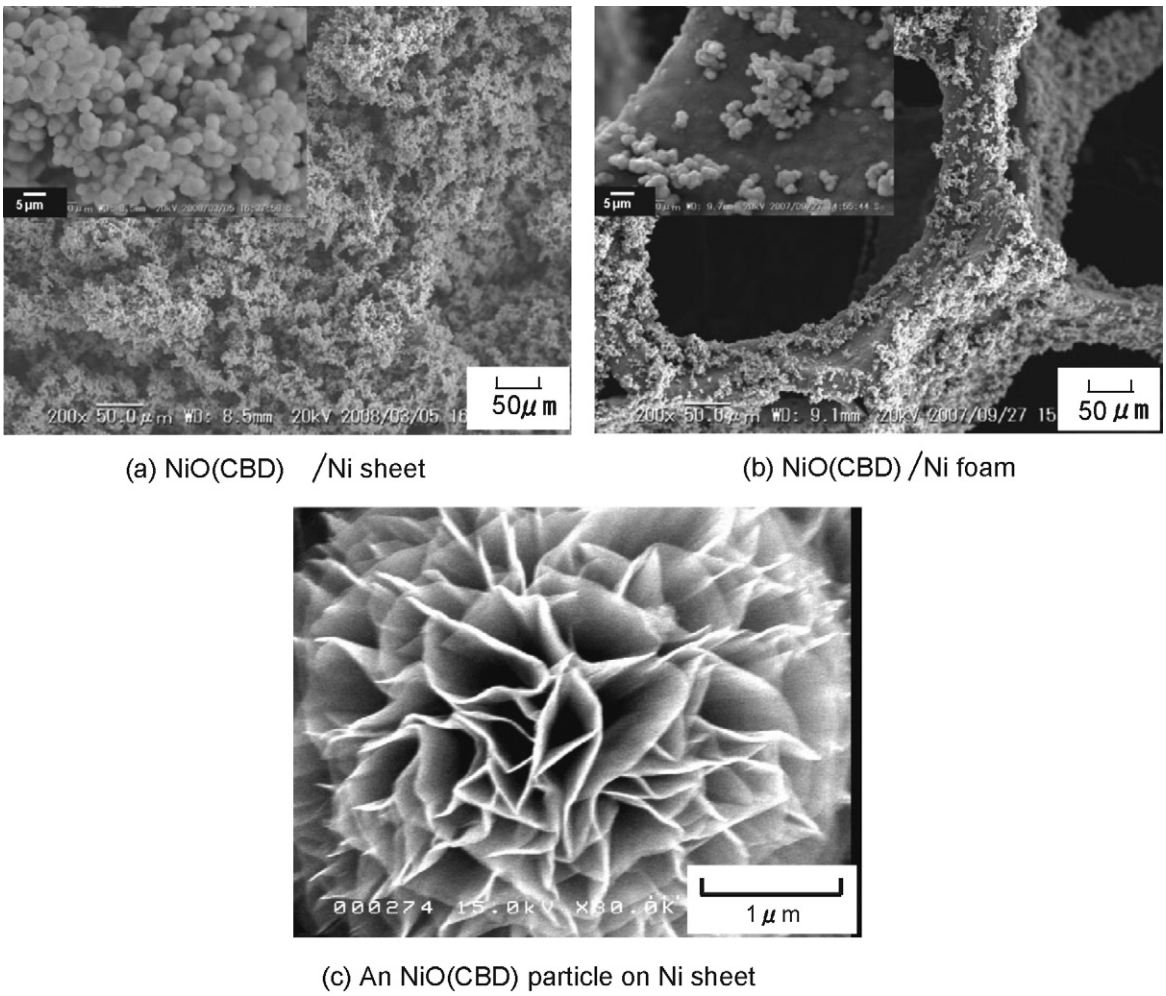

Fig. 3. SEM images for (a) NiO(CBD)/Ni sheet, (b) NiO(CBD)/Ni foam and (c) an NiO(CBD) particle on the Ni Sheet.

at 400 °C for 1 h. Diffraction peaks before the heat-treatment were well assigned to $Ni(OH)_2$(OH, S, H_2O)(JCPDS: 25-1363) whose XRD pattern was quite similar to α-phase $Ni(OH)_2$ [20], suggesting that OH^-, SO_4^{2-} and H_2O were intercalated between laminated $Ni(OH)_2$ sheets to expand an interlayer spacing. The SO_4^{2-} seems to come from persulfate, suggesting that the oxidation of $Ni(NH_3)_6^{2+}$ and/or $Ni(OH)_2$ by persulfate occurred, although some oxidation products like NiOOH were not clearly detected by XRD.

After the heat-treatment, the peaks assigned to $Ni(OH)_2$(OH, S, H_2O) disappeared and peaks assigned to rock salt NiO appeared at $2\theta = 37°$, 43° and 63° instead [21], clearly indicating that the $Ni(OH)_2$ was completely converted to NiO during the heat-treatment. The $Ni(OH)_2$(CBD)/Ni foam after the heat-treatment is named the NiO(CBD)/Ni foam hereafter.

XRD patterns for deposits on a Ni sheet before and after the heat-treatment were quite similar to those for the $Ni(OH)_2$(CBD)/Ni foam

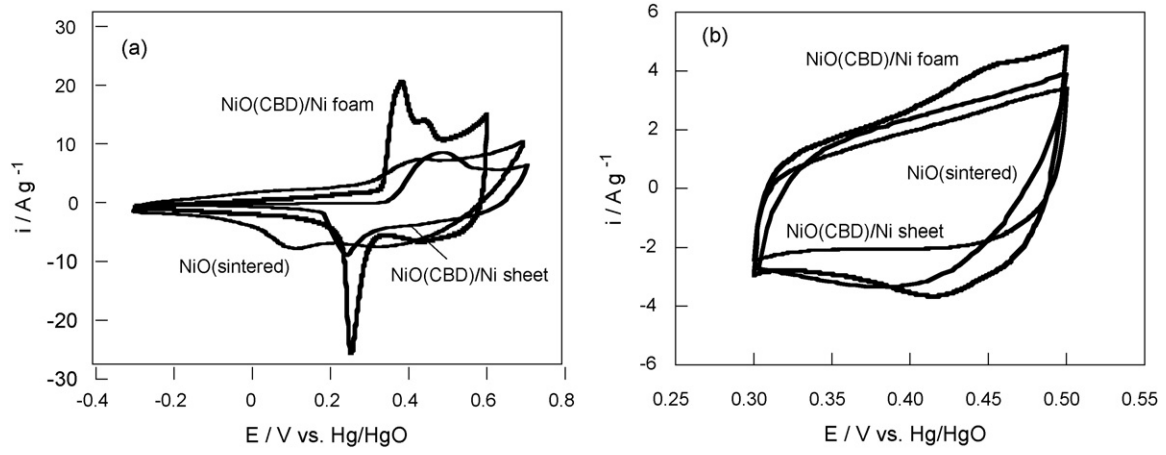

Fig. 4. Cyclic voltammograms of the NiO(CBD)/Ni foam, NiO(CBD)/Ni sheet and NiO(sintered) positive electrodes in the potential ranges of (a) −0.3 to 0.7 V and (b) 0.3–0.5 V in 10 M KOH aqueous solution. Sweep rate: 20 mV s^{-1}.

and NiO(CBD)/Ni foam, respectively, indicating that the structure of deposits was not influenced by substrate. So the $Ni(OH)_2$(CBD)/Ni sheet is transformed to the NiO(CBD)/Ni sheet after the heat-treatment.

Fig. 2 shows EDX spectra for deposits prepared by CBD on a Ni foam before and after heat-treatment at 400 °C for 1 h. Ni, O and S elements were detected in the EDX spectrum before the heat-treatment, indicating the production of $Ni(OH)_2$(OH, S, H_2O) by CBD. The S peak was detected even after the heat-treatment, suggesting that the S species have not been completely removed. EDX spectra for $Ni(OH)_2$(CBD)/Ni sheet before and after the heat-treatment were also quite similar to those for the $Ni(OH)_2$(CBD)/Ni foam, respectively.

SEM images of NiO(CBD)/Ni foam, NiO(CBD)/Ni sheet and an NiO particle on the Ni sheet are shown in Fig. 3. In Fig. 3(a) and (b), spherical NiO particles were loaded on both Ni substrates, and each particle had flower-like porous morphology which was composed of aggregated nanosheets, as shown in Fig. 3(c). The unique morphology had been formed during CBD and was maintained during the heat-treatment. The average size of NiO particles loaded on the Ni sheet and Ni foam was ca. 5 μm and ca. 2 μm, respectively. In addition, as can be seen from Fig. 3(a) and (b), the NiO particles on the Ni sheet are more packed than those on the Ni foam. So it can be expected that the latter has higher utilization of the positive active material than the former.

Fig. 4 shows cyclic voltammograms (CVs) of the NiO(CBD)/Ni foam, NiO(CBD)/Ni sheet and NiO(sintered) positive electrodes in 10 M KOH aqueous solution. Fig. 4(a) shows that at each electrode, a couple of redox peaks were observed, and can be assigned to the following reaction [22]:

$$NiO + OH^- = NiOOH + e^- \quad (4)$$

It is known that the electronic conductivity of NiOOH is higher than NiO and $Ni(OH)_2$. So once the NiOOH is formed, it should not be reduced to NiO as long as electrode potential is kept to 0.3 V vs. Hg/HgO and more, indicating that high electronic conductivity is maintained. As shown in Fig. 4(b), there were not distinct redox peaks in the potential range between 0.3 and 0.5 V at which oxygen evolution begins, suggesting that all CVs show a capacitive behavior. So the size of the AC negative electrode in each HC cell was controlled to move the potential at the positive electrode in the potential range between 0.3 and 0.5 V.

Figs. 5 and 6 show the change in cell voltage and potentials at the positive and negative electrodes in the HC cells with NiO(CBD)/Ni sheet (HC_{sheet}) and NiO(CBD)/Ni foam positive electrodes (HC_{foam}), respectively. The operating voltage for both HC cells was in the range of 0.8–1.5 V. The maximum cell voltage was much higher than that of a typical EDLC cell with two AC electrodes (0.9 V) and the HC cell with the previously used $Ni(OH)_2$ electrode (1.2 V) [6], and theoretical decomposition voltage of water (1.23 V). Moreover, in Figs. 4(b) and 5(b) the potentials at the positive and negative electrodes ran in the ranges of 0.3–0.5 V, in which NiOOH with higher electronic conductivity than NiO is the major species, and −1.0 to −0.5 V, respectively. The increase in cell voltage up to 1.5 V is ascribable to the expansion of potential range to cycle, particularly at the positive electrode.

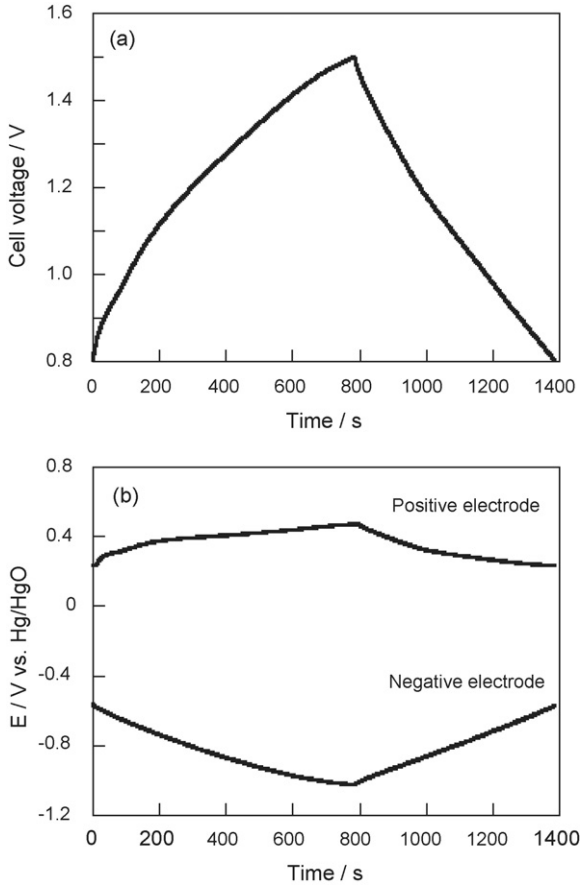

Fig. 6. Change in (a) cell voltage and (b) potentials at the positive and negative electrodes for the HC cell with the NiO(CBD)/Ni foam electrode in charge and discharge processes. Charge and discharge currents: 1 mA.

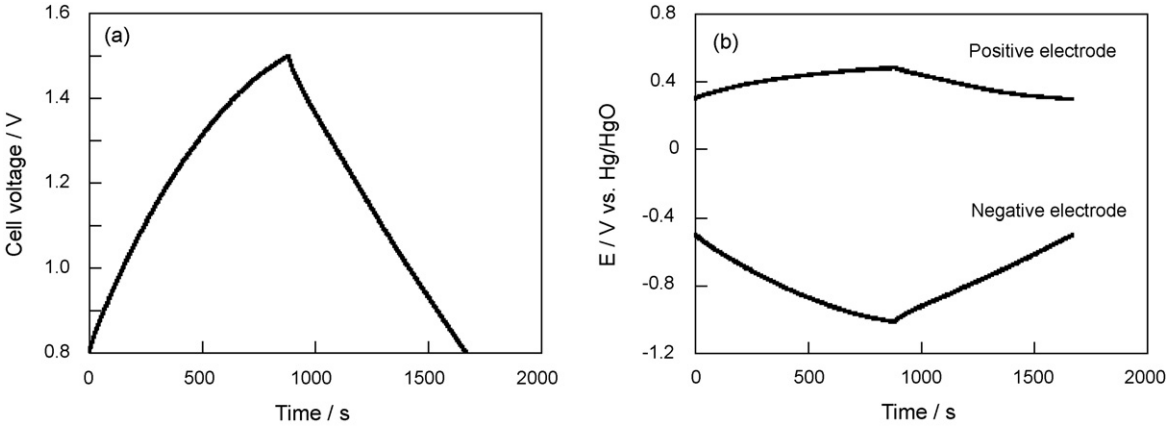

Fig. 5. Change in (a) cell voltage and (b) potentials at the positive and negative electrodes for the HC cell with the NiO(CBD)/Ni sheet electrode in charge and discharge processes. Charge and discharge currents: 1 mA.

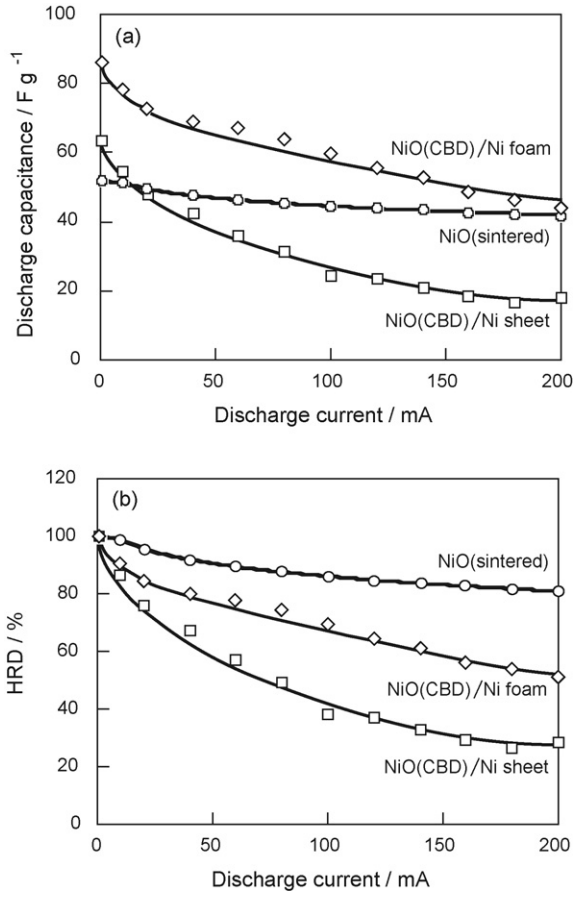

Fig. 7. (a) Discharge capacitance and (b) HRD as a function of discharge current for HC cells with NiO(CBD)/Ni sheet, NiO(CBD)/Ni foam and NiO(sintered) positive electrodes. Charge current: 1 mA.

Fig. 7 shows discharge capacitances and HRDs as a function of discharge current for the HC_{sheet}, HC_{foam} and the HC cell with the NiO(sintered) positive electrode ($HC_{sintered}$). In discharge capacitance at 1 mA, the HC_{sheet} and HC_{foam} were higher than the $HC_{sintered}$, suggesting that the utilization of the NiO(CBD)/Ni foam and NiO(CBD)/Ni sheet was higher than that of the NiO(sintered). Moreover, the HC_{foam} had higher discharge capacitance than the HC_{sheet}. However, the discharge capacitances and HRDs for the HC_{sheet} and HC_{foam} significantly decreased with an increase in discharge current, compared to the $HC_{sintered}$. Fig. 7(b) clearly demonstrates that the HRD decreases in the order of $HC_{sintered} > HC_{foam} > HC_{sheet}$.

Fig. 8 shows IR drops at various discharge currents for the HC cells with three positive electrodes. In all cases, IR drop linearly increased with discharge current. The IR drop increased in order of $HC_{sintered} < HC_{foam} < HC_{sheet}$. The cell resistance of each HC cell can be evaluated from a slope of each straight line in Fig. 7, and were 0.34 Ω for $HC_{sintered}$, 1.16 Ω for HC_{foam} and 1.43 Ω for HC_{sheet}. The NiO(sintered) was prepared by heat-treating a commercial sintered $Ni(OH)_2$ electrode. It is well-known that the sintered $Ni(OH)_2$ electrode includes Co species as an electronic conducting material, and their oxidation products form an electronic conducting network [23], leading to the increase in electronic conductivity or the decrease in IR drop. On the contrary, the NiO particles on the Ni foam is not so packed compared to those on the Ni sheet (see Fig. 3), leading to the lower IR drop. From Figs. 7 and 8, we can say that the smaller the IR drop, the higher the HRD.

Ragone plots for the HC cells with three positive electrodes are shown in Fig. 9(a). From the discharge curves at various discharge currents, energy and power densities per mass of both active materials were evaluated according to Ref. [12]. The energy density increased in order of $HC_{sintered} < HC_{sheet} < HC_{foam}$, while the power density increased in order of $HC_{sheet} < HC_{sintered} < HC_{foam}$. The HC_{foam} has relatively low cell resistance and small amount of NiO, leading to higher power density. The Ragone plots clearly indicate that the NiO(CBD)/Ni foam is the best positive electrode in the present study in terms of both energy and power densities.

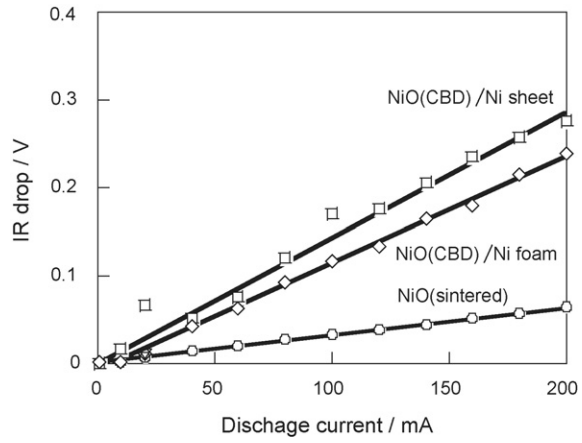

Fig. 8. IR drop as a function of discharge current for the HC cells with NiO(CBD)/Ni sheet, NiO(CBD)/Ni foam and NiO(sintered) positive electrodes. Charge current: 1 mA.

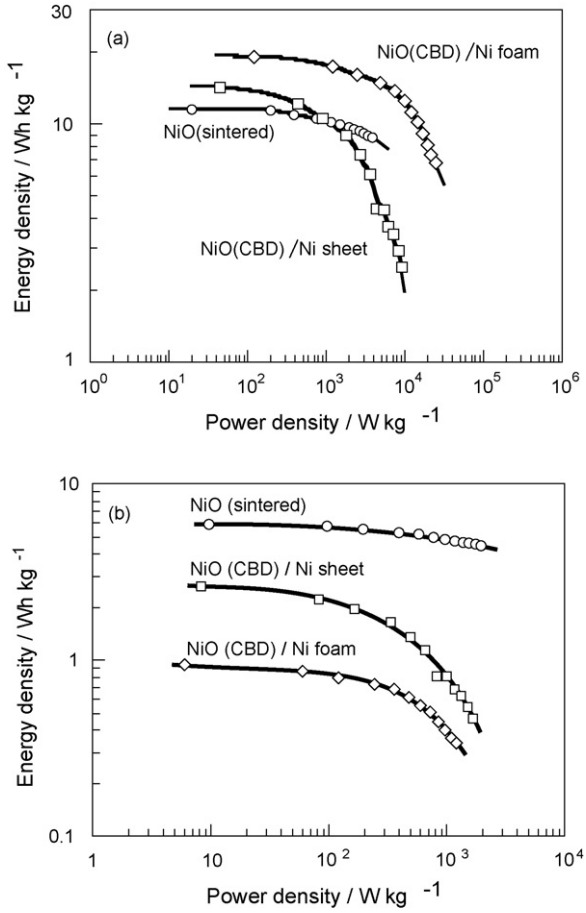

Fig. 9. Ragone plots per mass of active materials (a) and total mass of active materials and substrates (b) for the HC cells with NiO(CBD)/Ni sheet, NiO(CBD)/Ni foam and NiO(sintered) positive electrodes.

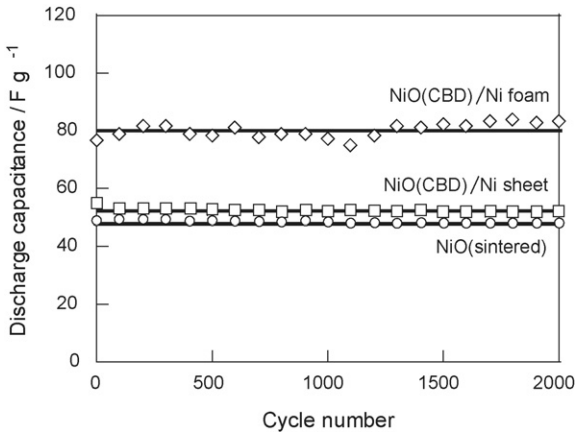

Fig. 10. Change in discharge capacitance with cycle number for the HC cells with NiO(CBD)/Ni sheet, NiO(CBD)/Ni foam and NiO(sintered) positive electrodes.

Fig. 9(b) also shows Ragone plots for the HC cells with three positive electrodes, but the energy and power densities are those per total mass of active materials and substrates. As can be seen from this figure, the energy and power densities for the HC_{sheet} and HC_{foam} were lower than those for the $HC_{sintered}$. However, it should be noticed that we have never optimized them in cases of the NiO(CBD)/Ni foam and NiO(CBD)/Ni sheet yet. So the energy and power densities for the HC_{sheet} and HC_{foam} will be still improved.

Fig. 10 shows the charge–discharge cycle performance of the HC cells with three positive electrodes at 2 mA. In all cases, the initial discharge capacitance was maintained even at 2000th cycle, indicating that all the HC cells have excellent cycle stability. This seems to come from high cycle stability of NiO positive active material, and in particular, the HC_{foam} can be an electrochemical capacitor with not only high energy and power densities but also high cycle stability.

4. Conclusion

We have prepared NiO particles on two types of Ni substrates by CBD and the following heat-treatment, and assembled HC cells with the NiO particles as the positive active material. The results obtained in the present study are summarized as follows.

(1) The NiO particles on the Ni sheet and Ni foam had flower-like porous morphology which was composed of aggregated nanosheets.

(2) The maximum operating voltage of both HC cells was 1.5 V, which was much higher than that of a typical EDLC cell (0.9 V), the HC cell with the sintered $Ni(OH)_2$ electrode (1.2 V) and the theoretical decomposition voltage of water (1.23 V).

(3) The HC_{foam} had higher discharge capacitance and high-rate dischargeability and lower IR drop than the HC_{sheet} because of the increase in the utilization of NiO active material.

(4) The Ragone plots showed that both energy and power densities for the HC_{foam} were much higher than those for the HC_{sheet} and $HC_{sintered}$, clearly indicating that the NiO(CBD)/Ni foam was the best positive electrode in the present study in terms of both energy and power densities.

(5) Both HC_{foam} and HC_{sheet} cells showed excellent cycle stability for 2000 cycles.

References

[1] B.E. Conway, Electrochemical Supercapacitors, Kluwer Academic/Plenum Publishers, New York, 1999.
[2] G.G. Amatucci, F. Badway, A. Du Pasquier, T. Zheng, J. Electrochem. Soc. 148 (2001) A930.
[3] A. Laforgue, P. Simon, J.F. Fauvarque, M. Mastragostino, F. Soavi, J.F. Sarrau, P. Lailler, M. Conte, E. Rossi, S. Saguatti, J. Electrochem. Soc. 150 (2003) A645.
[4] T. Brousse, R. Marchand, P.L. Taberna, P. Simon, J. Power Sources 158 (2006) 571.
[5] J.H. Park, O.O. Park, K.H. Shin, C.S. Jin, J.H. Kim, Electrochem. Solid-State Lett. 5 (2002) H7.
[6] S. Nohara, T. Asahina, H. Wada, N. Furukawa, H. Inoue, N. Sugoh, H. Iwasaki, C. Iwakura, J. Power Sources 157 (2006) 605.
[7] Y.G. Wang, L. Cheng, Y.Y. Xia, J. Power Sources 153 (2006) 191.
[8] M.S. Hong, S.H. Lee, S.W. Kim, Electrochem. Solid-State Lett. 5 (2002) A227.
[9] D. Villers, D. Jobin, C. Soucy, D. Cossement, R. Chahine, L. Breau, D. Belanger, J. Electrochem. Soc. 150 (2003) A747.
[10] T. Brousse, M. Toupin, D. Bélanger, J. Electrochem. Soc. 151 (2004) A614.
[11] V. Khomenko, E. Raymundo-Piñero, F. Béguin, J. Power Sources 153 (2006) 183.
[12] H. Inoue, T. Morimoto, S. Nohara, Electrochem. Solid-State Lett. 10 (2007) A261.
[13] H. Inoue, Y. Namba, E. Higuchi, S. Nohara, The 213th Electrochemical Society Meeting, Phoenix, 2008, Abstract No. 178.
[14] P. Pramanik, S. Bhattacharya, J. Electrochem. Soc. 137 (1990) 3869.
[15] S.-Y. Han, D.-H. Lee, Y.-J. Change, S.-O. Ryu, T.-J. Lee, C.-H. Change, J. Electrochem. Soc. 153 (2006) C382.
[16] M.A. Vidales-Hurtado, A. Mendoza-Galvan, Mater. Chem. Phys. 107 (2008) 33.
[17] U.M. Patil, R.R. Salunkhe, K.V. Gurav, C.D. Lokhande, Appl. Surf. Sci. 255 (2008) 2603.
[18] X.H. Xia, J.P. Tu, J. Zhang, X.H. Huang, X.L. Wang, W.K. Zhang, H. Huang, Electrochem. Commun. 10 (2008) 1815.
[19] H. Unuma, Y. Saito, K. Watanabe, M. Sugawara, Thin Solid Films 468 (2004) 4.
[20] P. Vishnu Kamath, M. Dixit, L. Indira, A.K. Shukla, V. Ganesh Kumar, N. Munichandraiah, J. Electrochem. Soc. 141 (1994) 2956.
[21] K.W. Nam, W.S. Yoon, K.B. Kim, Electrochim. Acta 47 (2002) 3201.
[22] K.-Y. Nam, K.-B. Kim, J. Electrochem. Soc. 149 (2002) A346.
[23] M. Oshitani, H. Yufu, K. Takashima, S. Tsuji, Y. Matsumura, J. Electrochem. Soc. 136 (1989) 1590.